

Dynamics of a charged particle around a weakly magnetized naked singularity

Gulmina Zaman Babar* and Mubasher Jamil†

*Department of Mathematics,
School of Natural Sciences,
National University of Sciences and Technology
Sector H-12, Islamabad, Pakistan*

Yen-Kheng Lim‡

*Department of Physics, National University of Singapore,
Singapore 117551, Singapore*

October 20, 2015

Abstract

We examine the motion of a charged particle in the vicinity of a weakly magnetized naked singularity. The escape velocity and energy of the particle moving around the naked singularity after being kicked by another particle or photon are investigated. Also at innermost stable circular orbit (ISCO) escape velocity and energy are examined. Effective potential and angular momentum of the particle are also discussed. We discuss the center of mass energy after collision between two particles having same mass and opposite charges moving along the same circular orbit in the opposite direction. It is investigated that under what conditions maximum energy can be produced as a result of collision.

*gulmina.zaman@sns.nust.edu.pk

†mjamil@sns.nust.edu.pk

‡phylyk@nus.edu.sg

1 Introduction

It is believed that particles in the surroundings of black holes are significantly influenced by the strong gravitational pull. Although, other forces that are usually supposed to be weaker are also at work near these objects. These include forces applied by the magnetic field and pressure of the infalling hot gases. Recent investigations have brought up the evidence that magnetic forces can be as powerful as gravity near supermassive black holes. But most of the work till now has been investigated for weak magnetic forces around black holes. The phenomenon of jet formation in black holes is widely under observation nowadays. Adequate amount of energy to establish and strengthen jets is yielded by the matter in accretion disk and rotation of the black hole. It is most likely believed that magnetic fields are responsible for the transfer of energy to the jets [1–3].

There are several papers that examine the dynamics of particles moving around weakly magnetized black holes. Motion of a charged particle near weakly magnetized Schwarzschild black hole is analyzed in [4–6]. The chaotic motion of a charged particle around Kerr black hole perturbed by magnetic field is investigated in [7–13]. Circular motion of charged particles around Reissner-Nordström spacetime is discussed in [14]. Chaotic particle motion in the Majumdar-Papapertou metric is discussed in [15, 16]. Furthermore, collision between particles and their escape energies after collision around Kiselev black hole [17] and a slowly rotating Kerr black hole [18] have been studied.

There are compelling arguments that black hole candidates in astrophysics could well be naked singularities instead of black holes, and that the distinction between the two possibilities may have observational consequences [19–21]. In this paper, we discuss motion of a charged particle around weakly magnetized naked singularity sourced by a massless scalar field. It is an extension of the Schwarzschild geometry when a massless scalar field is added to it which deforms the event horizon into a naked singularity. This solution was first discovered by Fisher [22], and subsequently rediscovered by Janis, Newman and Winicour [23] and others [24–26]. Subsequent works eventually show that some of these independently-found solutions are equivalent (see, e.g., Ref. [27]). This solution is known in literature as the Fisher solution, or the Janis-Newman-Winicour solution. The understanding of the physical properties and other features of this spacetime were expanded by Janis, Robinson and Winicour, [28]; therefore it is also sometimes known as the Fisher-Janis-Robinson-Winicour spacetime. A generalization to higher dimensions was given in [29], and an analysis of its properties in higher dimensions was performed by Abdolrahimi and Shoom [30]. More recently it was shown that this spacetime is isometric to a class of unique spacetimes possessing a photon sphere [31].

While this spacetime is known under many different names, for the purposes of this paper, we shall follow references related to the context of our paper such as [20, 32, 33] and refer to this solution as the Janis-Newman-Winicour (JNW) spacetime. The charged

generalization of this solution was obtained by Penney [34], and an exact magnetized solution was given by [35], and a further accelerating generalization was given in [36].

In [6] motion of a charged particle is discussed in the vicinity of weakly magnetized Schwarzschild black hole. The effect of the magnetic field on a charged particle is similar to the effect of the black hole rotation on a neutral particle. Like fast-rotating black holes weakly magnetized black holes behaves as particle accelerators. The case of particle motion around weakly magnetized Kerr black holes was considered recently in [37]. The critical escape energy and velocity of the kicked charged particle with different initial radial velocities have been investigated in [38]. Recently Lim studied the motion of charged particles around an electrified black hole [39].

Our core interest is to study the motion of a charged particle orbiting in the JNW spacetime after being hit by another particle. We are considering homogeneous magnetic field at spatial infinity. After collision the particle may pursue its motion in distinctive trajectories. We examine that, under what circumstances can a particle leave the locality of naked singularity and what causes the particle to fall in the naked singularity.

In Sec. 2, we derive the general equations of motion for a charged particle in a magnetized JNW spacetime. The equations will contain special cases that will be studied in subsequent sections. Particularly, in Sec. 3 we consider the special case of a particle in the absence of a magnetic field. The value of inner most stable circular orbit (ISCO) is investigated. Escape velocity of the particle is determined, also at the ISCO its value is computed. Energy of the particle is brought under analysis and its value at the ISCO is calculated. In Sec. 4, the motion of charged particles in weakly magnetized spacetimes are discussed. To simplify the analysis, dimensionless forms of the equations of motion, effective potential, energy and escape velocity are discussed. Dimensionless angular momentum and magnetic field are also investigated. In Sec. 5, we made an analysis of collision between two particles with same mass and opposite charges revolving around the naked singularity and computed the center-of-mass energy produced as a result of collision.

2 Particles in a magnetized JNW spacetime

2.1 Metric

We will be considering the motion of a charged particle in the magnetized JNW (or FJRW) spacetime [35]. This can be obtained by taking the ordinary JNW metric and applying a Harrison-type transformation [35, 40–42] to it. The result is an exact solution given by

the metric

$$\begin{aligned}
ds^2 &= \Lambda^2 (-f^\nu dt^2 + f^{-\nu} dr^2 + r^2 f^{1-\nu} d\theta^2) + \Lambda^{-2} r^2 f^{1-\nu} \sin^2 \theta d\phi^2, \\
f &= 1 - \frac{r_g}{r}, \quad \Lambda = 1 + \frac{1}{4} B^2 r^2 f^{1-\nu} \sin^2 \theta,
\end{aligned} \tag{1}$$

while the massless scalar field is given by

$$\varphi = \sqrt{\frac{1-\nu^2}{2}} \ln f, \tag{2}$$

and the Maxwell potential is

$$A = \frac{B r^2 f^{1-\nu} \sin^2 \theta}{2\Lambda} d\phi. \tag{3}$$

The Maxwell tensor accordingly is $F_{\mu\nu} = \partial_\mu A_\nu - \partial_\nu A_\mu$. It can be verified that the metric (1), together with (2) and (3) solves the four-dimensional Einstein-Maxwell-scalar equations.

The parameters r_g and ν are related to the black hole mass M and scalar charge q by

$$M = \frac{1}{2} \nu r_g, \quad q = \frac{1}{2} r_g \sqrt{1-\nu^2}, \tag{4}$$

while the parameter B is related to the strength of the axisymmetric magnetic field. We can see that the case $\nu = 1$ (or, equivalently, $q = 0$) reduces to the magnetic Ernst spacetime. On the other hand, for $B = 0$ we recover the usual JNW spacetime. Setting both $B = 0$ and $\nu = 1$ gives the Schwarzschild spacetime. Similar to the unmagnetized case, the metric (1) has a strong curvature singularity at $r = r_g$. Similar to the Ernst solution, this solution is not asymptotically flat.

2.2 Equations of motion

For a test particle of charge per unit mass e , its motion is described by a trajectory $x^\mu(\tau)$, where τ is an appropriate affine parametrization. The motion is determined by the Lagrangian $L = \frac{1}{2} g_{\mu\nu} \dot{x}^\mu \dot{x}^\nu + e A_\mu \dot{x}^\mu$, where overdots denote derivatives with respect to τ . The equations of motion satisfied by $x^\mu(\tau)$ can be derived with the Euler-Lagrange equations $\frac{d}{d\tau} \frac{\partial L}{\partial \dot{x}^\mu} = \frac{\partial L}{\partial x^\mu}$.

In the following, it will be convenient to define

$$F \equiv f^\nu, \quad G \equiv f^{1-\nu}, \tag{5}$$

such that the Lagrangian describing a charged particle in the magnetized JNW spacetime

is given by

$$L = \frac{1}{2} \left[\Lambda^2 \left(-F\dot{t}^2 + \frac{\dot{r}^2}{F} + r^2 G \dot{\theta}^2 \right) + \frac{r^2 G \sin^2 \theta}{\Lambda^2} \dot{\phi}^2 \right] + \frac{eBr^2 G \sin^2 \theta}{2\Lambda} \dot{\phi}. \quad (6)$$

Since the Lagrangian is cyclic in t and ϕ , we have the following first integrals

$$\dot{t} = \frac{\mathcal{E}}{\Lambda^2 F}, \quad \dot{\phi} = \frac{\Lambda^2}{r^2 G \sin^2 \theta} \left(\mathcal{L} - \frac{eBr^2 G \sin^2 \theta}{2\Lambda} \right), \quad (7)$$

where \mathcal{E} and \mathcal{L} are conserved quantities which we may interpret as the energy and angular momentum of the particle, respectively. Applying the Euler-Lagrange equation to the remaining two coordinates gives

$$\begin{aligned} \ddot{r} = & \left(\frac{F'}{2F} - \frac{\partial_r \Lambda}{\Lambda} \right) \dot{r}^2 + FG \left(r + \frac{r^2 \partial_r \Lambda}{\Lambda} + \frac{r^2 G'}{2G} \right) \dot{\theta}^2 - \frac{2\partial_\theta \Lambda}{\Lambda} \dot{r} \dot{\theta} \\ & + \frac{F}{r^3 G \sin^2 \theta} \left(1 - \frac{r \partial_r \Lambda}{\Lambda} + \frac{r G'}{2G} \right) \left(\mathcal{L} - \frac{eBr^2 G \sin^2 \theta}{2\Lambda} \right)^2 \\ & + \frac{eBF}{r\Lambda} \left(1 - \frac{r \partial_r \Lambda}{2\Lambda} + \frac{r G'}{2G} \right) \left(\mathcal{L} - \frac{eBr^2 G \sin^2 \theta}{2\Lambda} \right) - \left(\frac{\partial_r \Lambda}{\Lambda} + \frac{F'}{2F} \right) \frac{\mathcal{E}^2}{\Lambda^4}, \end{aligned} \quad (8)$$

$$\begin{aligned} \ddot{\theta} = & \frac{\partial_\theta \Lambda}{\Lambda} \left(\frac{\dot{r}^2}{Fr^2 G} - \dot{\theta}^2 \right) - 2 \left(\frac{\partial_r \Lambda}{\Lambda} + \frac{1}{r} + \frac{G'}{2G} \right) \dot{r} \dot{\theta} - \frac{\mathcal{E}^2 \partial_\theta \Lambda}{\Lambda^5 F r^2 G} \\ & + \frac{1}{r^4 G^2 \sin^3 \theta} \left(\cos \theta - \frac{\sin \theta \partial_\theta \Lambda}{\Lambda} \right) \left(\mathcal{L} - \frac{eBr^2 G \sin^2 \theta}{2\Lambda} \right)^2 \\ & + \frac{eB}{\Lambda r^2 G \sin \theta} \left(\cos \theta - \frac{\sin \theta \partial_\theta \Lambda}{2\Lambda} \right) \left(\mathcal{L} - \frac{eBr^2 G \sin^2 \theta}{2\Lambda} \right). \end{aligned} \quad (9)$$

Here, the primes appearing in F' and G' denote derivatives with respect to r . The invariance of $g_{\mu\nu} \dot{x}^\mu \dot{x}^\nu \equiv \epsilon$ gives a constraint equation

$$-\frac{\mathcal{E}^2}{\Lambda^2 F} + \frac{\Lambda^2}{r^2 G \sin^2 \theta} \left(\mathcal{L} - \frac{eBr^2 G \sin^2 \theta}{2\Lambda} \right)^2 + \Lambda^2 \left(\frac{\dot{r}^2}{F} + r^2 G \dot{\theta}^2 \right) = \epsilon. \quad (10)$$

By appropriately rescaling the affine parameter τ , the magnitude of ϵ can be set to unity if it is nonzero. Therefore in the following, we have $\epsilon = -1$ for timelike particles and $\epsilon = 0$ for photons or null geodesics. The equations of motion (8) and (9), together with the constraint (10) contains various special cases for motion in related spacetimes. For instance, setting $\nu = 1$ describes the motion in the magnetic Ernst spacetime studied in Refs. [39, 43–45]. Setting $B = 0$ will give the geodesic equations in the JNW spacetime, and finally if $\nu = 1$ and $B = 0$ we have the well-known equations for Schwarzschild geodesics.

The constraint equation (10) can be also cast in the effective potential formulation

$$\Lambda^4 \left(\dot{r}^2 + r^2 F G \dot{\theta}^2 \right) = \mathcal{E}^2 - \mathcal{U}^2, \quad (11)$$

where

$$\mathcal{U}^2 = \frac{\Lambda^4 F}{r^2 G \sin^2 \theta} \left(\mathcal{L} - \frac{e B r^2 G \sin^2 \theta}{2 \Lambda} \right)^2 - \epsilon \Lambda^2 F. \quad (12)$$

While in general, the effective potential \mathcal{U}^2 is a complicated function that depends on parameters \mathcal{L} , ν , B and r_g , we can make a few qualitative observations.

Firstly, we note the asymptotic behavior of \mathcal{U}^2 , at large r , is

$$\mathcal{U}^2 \sim \frac{1}{256} B^6 (r \sin \theta)^6 (\mathcal{L} B - 2e)^2 + \mathcal{O}(r^5). \quad (13)$$

Thus, at large distances away from the singularity, the potential increases to the order of $(r \sin \theta)^6$. Therefore, for large values of r where $r \rightarrow \infty$, the potential remains finite if $\theta \rightarrow 0$ or π . Thus a particle with finite energy \mathcal{E} can escape to infinity if the trajectory takes it along a path close to the polar axis $\theta = 0$ or $\theta = \pi$.

Secondly, at distances close to the $r = r_g$ singularity, due to the factor $F/G = f^{2\nu-1}$ in front of the paranthesis in (12), we have

$$\lim_{r \rightarrow r_g^+} \mathcal{U}^2 = \begin{cases} 0, & \text{if } \nu > \frac{1}{2}, \\ +\infty & \text{if } \nu < \frac{1}{2} \text{ and } \left(\mathcal{L} - \frac{e B r^2 G \sin^2 \theta}{2 \Lambda} \right) \neq 0. \end{cases} \quad (14)$$

Therefore for $\nu < \frac{1}{2}$ and $\left(\mathcal{L} - \frac{e B r^2 G \sin^2 \theta}{2 \Lambda} \right) \neq 0$ there exist an infinite potential barrier preventing the particle from reaching the $r = r_g$ singularity.

2.3 Equatorial circular orbits

We can easily check that $\theta = \pi/2$ is a trivial solution to Eq. (9), where $\ddot{\theta} = \dot{\theta} = 0$. These orbits lie in the equatorial plane. The plots of \mathcal{U}^2 against r for various cases are shown in Fig. (1).

For the unmagnetized case $B = 0$, the effective potential obtained in [32] is reproduced. In particular, for $\nu < \frac{1}{2}$ the potential becomes an infinite barrier. Now if the magnetic field is turned on, an additional gravitational attraction is provided by the magnetic field itself, manifesting in a potential well. Thus charged particles in the magnetized JNW spacetime is bound more tightly compared to the unmagnetized case.

For concreteness, we will be mainly interested in a charged particles which are initially in the innermost stable circular orbit (ISCO), while second particle is coming from infinity. They both collide in the ISCO. We may define circular orbits to be those of constant r

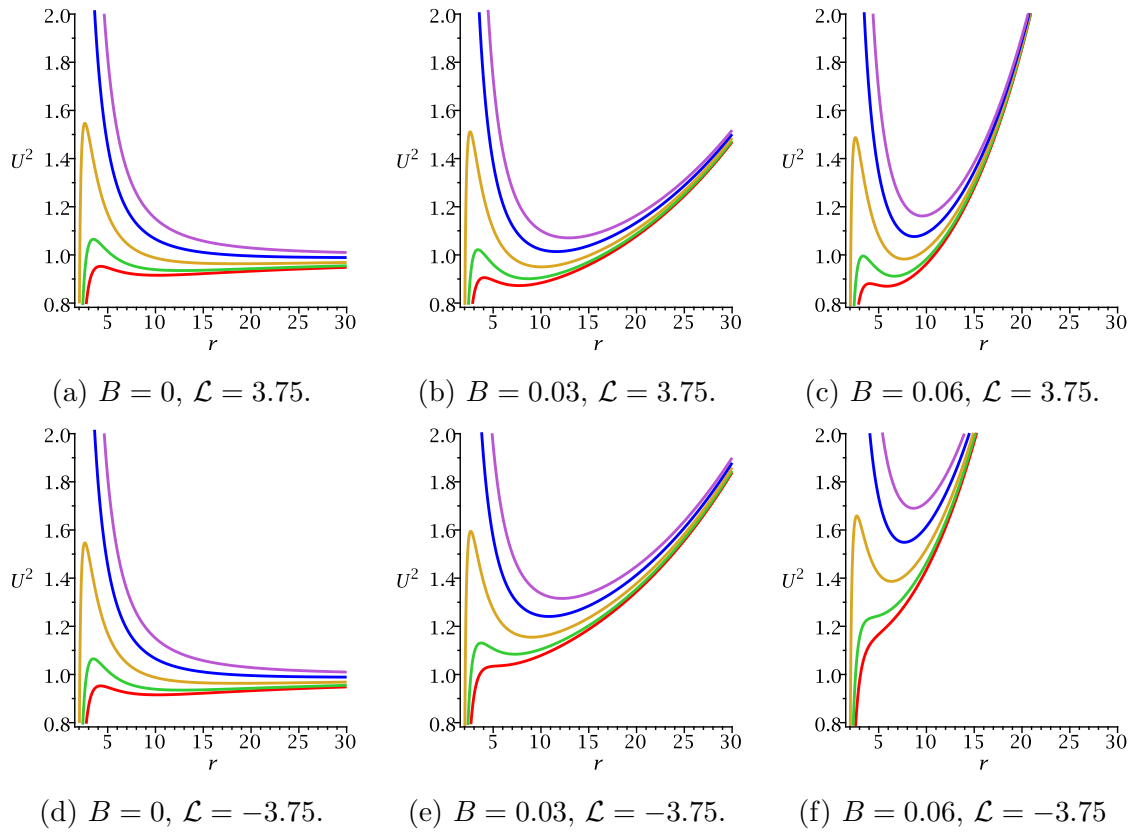


Figure 1: (Color online) Plots of \mathcal{U}^2 vs r at $\theta = \pi/2$ and $r_g = 2$ for timelike ($\epsilon = -1$) particles of charge $e = 1$, with various values of B and \mathcal{L} . Each plot contains curves of various values of ν , from bottom to the top, $\nu = 1, 0.9, 0.7, 0.5$ and 0.3 .

and θ . We seek such orbits exist in the equatorial plane where θ is a constant equal to $\pi/2$, thus Eq. (9) is automatically satisfied. By demanding that $r = r_o$ is a constant in (8) and (10), we have,

$$\mathcal{L}_{\pm} = \frac{2r_o G \left[eBr_o^2 G (6B^2 r_o FG + 3B^2 r_o^2 FG' + F'(4 + B^2 r_o^2 G)) \pm \sqrt{K} \right]}{(4 + B^2 r_o^2 G) [(3B^2 r_o^2 G - 4)(2G + r_o G')F + r_o GF'(4 + B^2 r_o^2 G)]}, \quad (15)$$

$$\begin{aligned} \mathcal{E}_{\pm}^2 &= \frac{F(4 + B^2 r_o^2 G)^2}{256r_o^2 G} \\ &\times \left[(4 + B^2 r_o^2 G)^2 \mathcal{L}_{\pm}^2 - 4eBG r_o^2 (4 + B^2 r_o^2 G) \mathcal{L}_{\pm} + 4Gr_o^2 (e^2 B^2 r_o^2 G - 4\epsilon) \right], \quad (16) \end{aligned}$$

where

$$\begin{aligned} K &= 2B^2 r_o^2 (2G + r_o G')^2 (3r_o^2 G \epsilon B^2 - 4\epsilon + 2e^2) F^2 \\ &+ \epsilon r_o F' (4 + B^2 r_o^2 G) (5B^2 r_o^2 G - 4) (2G + r_o G') F + r_o^2 G F'^2 \epsilon (4 + B^2 r_o^2 G)^2 \quad (17) \end{aligned}$$

We consider the stability of a circular orbit by perturbing about the radius r_o by writing

$$r(\tau) = r_o + \epsilon r_1(\tau). \quad (18)$$

We substitute this into Eq. (8). To first order in ϵ , the equations of motion reduce to

$$\ddot{r}_1 = -\omega^2 r_1, \quad (19)$$

where, in general, the expression for ω is a complicated function of ν , B , r_g and r_o that is too complicated to be shown here, however it can be handled straightforwardly using a standard computer algebra software such as MAPLE.

We can, however, study the qualitative behavior of ω^2 for various spacetime and orbital parameters. Fig. (2) shows the values of ω^2 for various B and ν . The circular orbits are stable for $\omega^2 > 0$, and we can see that for the case $B = 0$ and $\nu = 1$ (the solid curve in Fig. (2a)) show that the stable circular orbits exist for $r_o > 3r_g$. This is the well-known case of circular orbits in the Schwarzschild spacetime.

Turning on the magnetic field, while keeping $\nu = 1$ corresponds to circular orbits in the magnetic Ernst spacetime. We see that the effect of the magnetic field brings the stable range of circular orbits closer to the black hole. (See the dotted, dashed and dash-dotted curves in Fig. (2a) and (2d)).

Setting $\nu < 1$, we see that spacetimes with a massless scalar field can support stable circular orbits of even smaller radii, in particular, for $\nu < 1/2$ all circular orbits up to those infinitesimally close to the singularity $r = r_g$ are stable. This is due to the existence of the infinite potential barrier, as shown in (14).

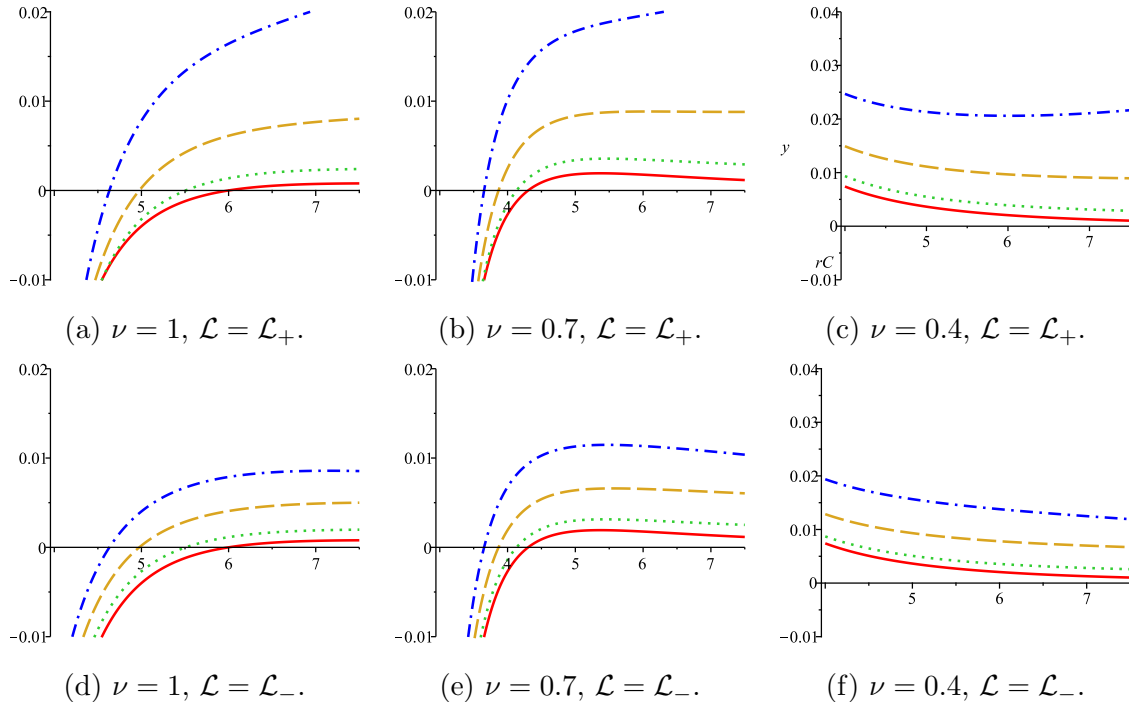


Figure 2: (Color online) Plots of ω^2 vs r_0 , for $e = 1$ and various ν in units where $r_g = 2$. For each value of ν , the solid, dotted, dashed and dash-dotted curves respectively correspond to $B = 0, 0.025, 0.05$, and 0.75 .

2.4 Escape trajectories

We consider particles initially in an ISCO which subsequently collides with another particle. In general, the collision would alter its energy and angular momentum, as well as its radial and angular velocities. For concreteness and simplicity, we restrict our attention to collision which only changes the energy of the particle, while the angular momentum remains the same. Furthermore, we assume that the radial velocity remains unchanged, therefore, $\dot{r} = 0$ after collision. From (10), this restricts us to the fact that increasing the energy results $\dot{\theta} \neq 0$, i.e., the particle gets kicked out from the equatorial plane.

Plotting the curves of $\mathcal{U}^2 = \mathcal{E}^2$ shows the boundary of regions accessible to the particle after collision. To demonstrate a specific example, we consider particles kicked from an ISCO in a spacetime of $B = 0.005$, $\nu = 0.9$, $r_g = 2$ and $e = 10$. Choosing the lower sign in (15), and solving for $\omega^2 = 0$ using Eq.(19), we find that the initial ISCO radius is $r_{(\text{ISCO})} = 4.9490145$, and the angular momentum and energy are respectively $\mathcal{L}_{-(\text{ISCO})} = 2.986451488$ and $\mathcal{E}_{(\text{ISCO})} = 0.8853807128$. With these parameters the curves in $\mathcal{U}^2 = \mathcal{E}^2$ are plotted in Cartesian-type coordinates projected on a plane where $\phi = 0$, (or, $y = 0$).

The dark regions in Figs. (3a)–(3d) indicate regions inaccessible to the particle. In particular, note that Figs. (3c) and (3d) shows that the particle has the ability to escape far from the origin if it travels up or down where $|z| \gg 1$. Recalling that, at $\phi = 0$,

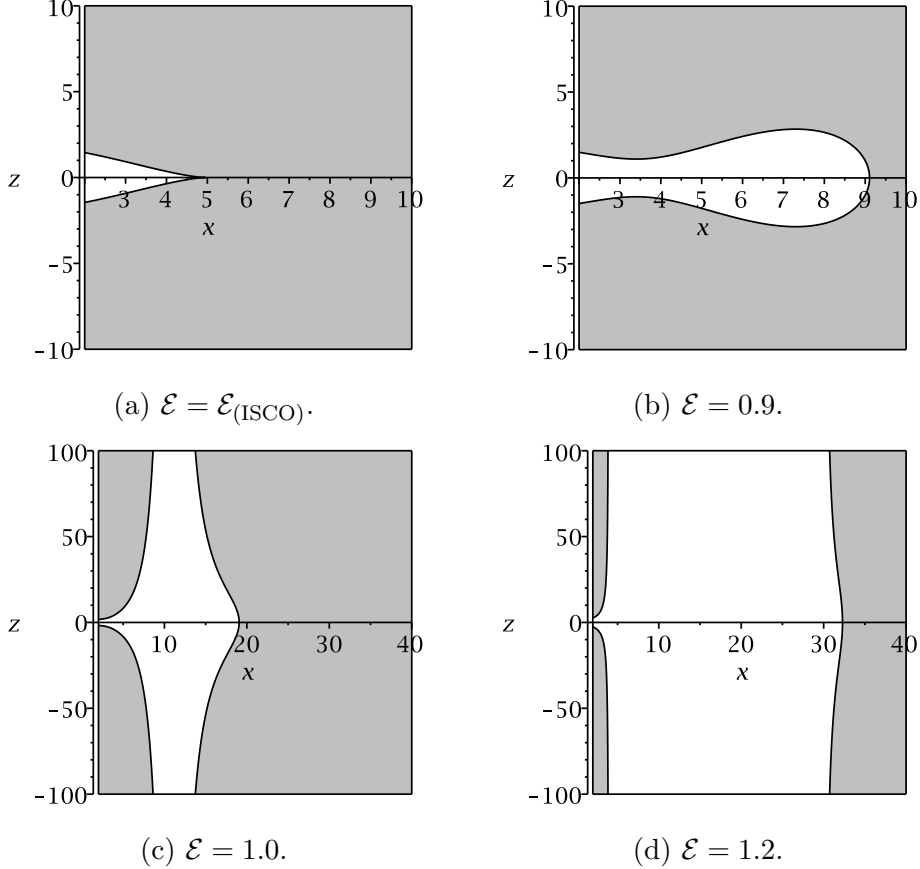
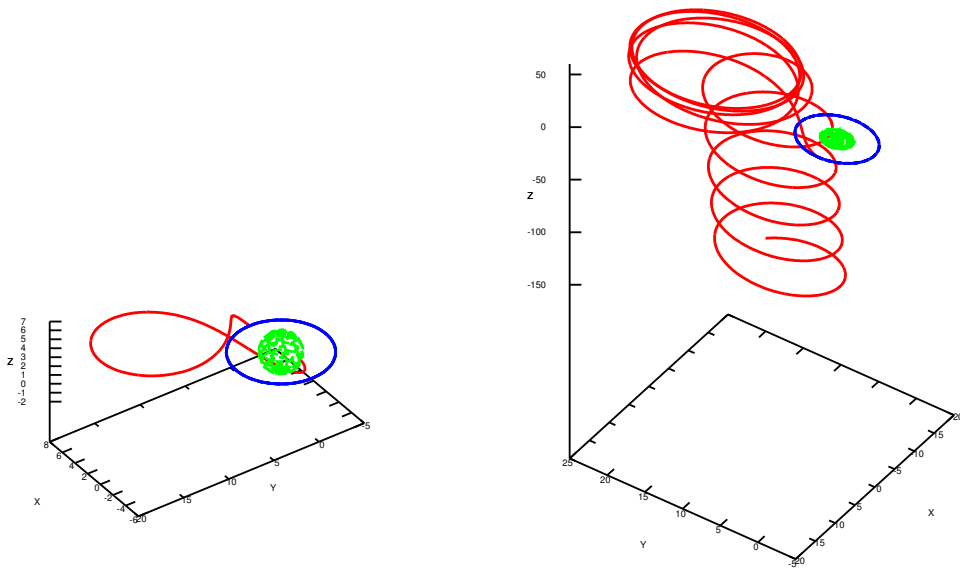


Figure 3: (Color online) Curves of $\mathcal{U}^2 = \mathcal{E}^2$ plotted as the boundary separating the regions accessible (white) and inaccessible (shaded) for a particle kicked from an ISCO into various possible energies. The spacetime parameters are $B = 0.005$, $\nu = 0.9$ and $r_g = 2$, and the charge per unit mass of the particle is $e = 10$. The initial ISCO radius for these spacetime parameters is $r_{\text{ISCO}} = 4.9490145$, as can be calculated from (19). The corresponding angular momentum is $\mathcal{L}_{-\text{ISCO}} = 2.986451488$.

we have $z = r \sin \theta$, hence this is consistent with the observation made in Eq. (14). The actual trajectory of a kicked particle may be obtained by integrating Eqs. (8) and (9) numerically. Continuing the example where $B = 0.005$, $\nu = 0.9$, $r_g = 2$ and $\mathcal{L}_{-\text{ISCO}}$, we track the motion of the particle after being kicked from the initial orbit at $r = r_{\text{ISCO}}$ into a new energy \mathcal{E} , with the angular momentum remaining the same and $\dot{r} = 0$ just after collision. The initial value of $\dot{\theta}$ just after collision is calculated from (10). With these initial conditions, we plot the trajectories for two possible values of $\mathcal{E} = 1.0$ and $\mathcal{E} = 1.1$, shown in Fig. (4).

As we can see, the particle after the kick may possibly fall into the $r = r_g$ singularity, as shown in Fig. (4a), or escape, shown in Fig. (4b) while continuing to execute a cyclotron-like spiral due to the Lorentz interaction with the magnetic field.



(a) $\mathcal{E} = 1.0$.

(b) $\mathcal{E} = 1.1$.

Figure 4: (Color online) Trajectory of a particle kicked from an initial ISCO orbit where $B = 0.005$, $\nu = 0.9$, $r_g = 2$, $e = 10$ and $|\mathcal{L}_{-(\text{ISCO})}| = 2.986451488$, for post-collision energies of $\mathcal{E} = 1.0$ and $\mathcal{E} = 1.1$. The sphere indicates the surface of the singularity $r = r_g = 2$, and the blue circles denote the particle's original ISCO orbit ($r_{\text{ISCO}} = 4.9490145$) before the collision.

3 Escape velocity in the unmagnetized JNW space-time

In this section, we consider the unmagnetized case where $B = 0$. The angular momentum and energy representing circular orbits, Eq. (15) and (16) for $B = 0$ are

$$\mathcal{L}_o = r_o \sqrt{\frac{\nu \left(1 - \frac{r_g}{r_o}\right)^{1-\nu} r_g}{2r_o - (1+2\nu)r_g}}, \quad \mathcal{E}_o = \sqrt{\left(1 - \frac{r_g}{r_o}\right)^\nu \left(\frac{2r_o - r_g(1+\nu)}{2r_o - r_g(1+2\nu)}\right)}. \quad (20)$$

For $\nu = 1/2$, the orbit exists for $r_o \in (\frac{3}{2}r_g, \infty)$ and the ISCO is specified by $r_o = \frac{3}{2}r_g$, which corresponds to an inflection point of the effective potential. For the ISCO we have

$$\mathcal{E}_{ISCO} = \frac{3^{\frac{1}{4}}}{\sqrt{2}}, \quad |\mathcal{L}_{zISCO}| = \frac{3^{\frac{3}{4}}}{2\sqrt{2}}r_g. \quad (21)$$

As already described in Sec. 2.4, we consider collision of particles initially in an ISCO with another particle, where we assume $\dot{r} = 0$ after the collision and \mathcal{L} remains unaltered, and the motion is mainly determined by the energy \mathcal{E} after the collision. Since this implies $\dot{\theta} \neq 0$ after the collision, the particles obtains a velocity $v_\perp = r\dot{\theta}$ ($\dot{\theta}_o$ is the initial polar angular velocity) in the direction orthogonal to the equatorial plane. The energy then takes the form

$$\mathcal{E} = \sqrt{\mathcal{E}_o^2 + v_\perp^2 \left(1 - \frac{r_g}{r_o}\right)}, \quad (22)$$

If $\mathcal{E} < 1$ particle cannot escape to infinity, it will escape to infinity if $\mathcal{E} \geq 1$ or in other words it will have unbounded motion,

$$v_\perp \geq \sqrt{(1 - \mathcal{E}_o^2) \left(\frac{r_o}{r_o - r_g}\right)}. \quad (23)$$

Specifically, for ISCO the escape condition for $\nu = \frac{1}{2}$ is, $|v_\perp| \geq v_\perp^{esc} \geq \sqrt{3 \left(1 - \frac{\sqrt{3}}{2}\right)}$.

4 Particles in a weakly magnetized JNW spacetime

4.1 Equations of motion in the weak magnetization regime

If the magnetic field is sufficiently weak such that they do not influence the particle gravitationally, there is a possibility for a particle to escape after collision. This may occur if $\Lambda \rightarrow 1$, or, equivalently, $B \rightarrow 0$. Nevertheless, the magnetic field may still influence the particle via the Lorentz force, as the coupling depends on eB . Thus, even for small B , the Lorentz force will remain significant for sufficiently large e .

Therefore, for timelike particles ($\epsilon = -1$), we shall focus on this weak magnetization regime by defining $B = \beta/e$ and expand the equations of motion (8) and (9) in powers of $1/e$, the result is

$$\ddot{r} = \frac{\nu r_g}{2r(r-r_g)} \dot{r}^2 + \frac{1}{2} (2r - r_g(1+\nu)) \dot{\theta}^2 - \frac{\nu r_g \mathcal{E}^2}{2r(r-r_g)} + \left(\frac{r-r_g}{r} \right)^{2\nu} \frac{[2r - r_g(1+\nu)] \mathcal{L}^2}{2(r-r_g)^2 r^2 \sin^2 \theta} + \mathcal{O}(1/e^2), \quad (24)$$

$$\ddot{\theta} = -\frac{2r - r_g(1+\nu)}{r(r-r_g)} \dot{r} \dot{\theta} + \left(\frac{r-r_g}{r} \right)^{2\nu} \frac{\mathcal{L}^2 \cos \theta}{r^2 (r-r_g)^2 \sin^3 \theta} - \frac{\beta^2}{4} \cos \theta \sin \theta + \mathcal{O}(1/e^2), \quad (25)$$

and the constraint equation becomes

$$0 = -\frac{\mathcal{E}^2}{F} + \frac{\mathcal{L}^2}{r^2 G \sin^2 \theta} - \beta \mathcal{L} + \frac{\dot{r}^2}{F} + r^2 G \dot{\theta}^2 + 1 + \frac{\beta^2}{4} r^2 G \sin^2 \theta + \mathcal{O}(1/e^2). \quad (26)$$

Substituting Eq. (26) into (24), and expressing the quantities in terms of f , we obtain

$$\ddot{r} = \frac{1}{2} (2r - (1+2\nu)r_g) \left(\dot{\theta}^2 + \frac{\mathcal{L}^2}{r^4 f^{2(1-\nu)} \sin^2 \theta} \right) + \frac{\nu r_g}{2r^2 f^{1-\nu}} (\beta \mathcal{L} - 1) - \frac{\beta^2}{8} (2r - r_g) \sin^2 \theta, \quad (27)$$

$$\ddot{\theta} = -\frac{2}{r} \left(1 + (1-\nu) \frac{r_g}{2rf} \right) \dot{r} \dot{\theta} + \frac{\mathcal{L}^2 \cos \theta}{r^4 f^{2(1-\nu)} \sin^3 \theta} - \frac{\beta^2}{4} \sin \theta \cos \theta. \quad (28)$$

Accordingly, to first-order in $1/e$, Eq. (7) reduces to

$$\mathcal{E} = f^\nu \dot{t}, \quad \mathcal{L} = \left(\dot{\phi} + \frac{\beta}{2} \right) r^2 f^{1-\nu} \sin^2 \theta. \quad (29)$$

Rearranging Eq. (26) we obtain an effective potential equation for the test field case

$$\mathcal{E}^2 = \dot{r}^2 + r^2 f \dot{\theta}^2 + U_{\text{eff}}, \quad U_{\text{eff}} = f^\nu \left[1 + r^2 f^{(1-\nu)} \sin^2 \theta \left(\frac{\mathcal{L}}{r^2 f^{(1-\nu)} \sin^2 \theta} - \frac{\beta}{2} \right)^2 \right]. \quad (30)$$

4.2 Dimensionless form of the equations

Following dimensionless quantities are introduced to avoid complications in our analysis regarding motion of the particle after collision,

$$\sigma = \frac{\tau}{r_g}, \quad \rho = \frac{r}{r_g}, \quad \ell = \frac{\mathcal{L}_z}{r_g}, \quad b = \frac{1}{2} \beta r_g, \quad \mathcal{T} = \frac{t}{r_g}. \quad (31)$$

The ρ and θ components of the dynamical equations (27) and (28) are expressed as follows:

$$\begin{aligned} \frac{d^2\rho}{d\sigma^2} &= \frac{1}{2}(2\rho - (1 + 2\nu)) \left(\frac{d\theta}{d\sigma}\right)^2 + \frac{\ell^2(2\rho - (1 + 2\nu))}{2\rho^4 \sin^2\theta \left(1 - \frac{1}{\rho}\right)^{2(1-\nu)}} + \\ &\frac{\nu}{2\rho^2 \left(1 - \frac{1}{\rho}\right)^{(1-\nu)}}(2\ell b - 1) - \frac{b^2}{2} \sin^2\theta(2\rho - 1), \end{aligned} \quad (32)$$

$$\begin{aligned} \frac{d^2\theta}{d\sigma^2} &= -\frac{2}{\rho} \frac{d\theta}{d\sigma} \frac{d\rho}{d\sigma} - \frac{(1-\nu)}{\rho^2 \left(1 - \frac{1}{\rho}\right)} \frac{d\theta}{d\sigma} \frac{d\rho}{d\sigma} + \frac{\ell^2 \cos\theta}{\rho^4 \sin^3\theta \left(1 - \frac{1}{\rho}\right)^{2(1-\nu)}} \\ &- b^2 \sin\theta \cos\theta, \end{aligned} \quad (33)$$

where the energy \mathcal{E} is

$$\mathcal{E}^2 = \left(\frac{d\rho}{d\sigma}\right)^2 + \rho(\rho - 1) \left(\frac{d\theta}{d\sigma}\right)^2 + U_{\text{eff}}, \quad (34)$$

and

$$U_{\text{eff}} = \left(1 - \frac{1}{\rho}\right)^\nu + \rho^2 \left(1 - \frac{1}{\rho}\right) \sin^2\theta \left(\frac{\ell}{\rho^2 \sin^2\theta \left(1 - \frac{1}{\rho}\right)^{1-\nu}} - b\right)^2. \quad (35)$$

When we consider the equatorial plane, then the particle moving around the naked singularity in the ISCO has the following energy,

$$\mathcal{E}_o^2 = \left(1 - \frac{1}{\rho_o}\right)^\nu + \rho_o^2 \left(1 - \frac{1}{\rho_o}\right) \left(\frac{\ell}{\rho_o^2 \left(1 - \frac{1}{\rho_o}\right)^{1-\nu}} - b\right)^2. \quad (36)$$

After the collision the motion of particle is merely determined by its new energy

$$\mathcal{E} = \sqrt{\mathcal{E}_o^2 + \frac{(\rho_o - 1)}{\rho_o} v_\perp^2}. \quad (37)$$

The particle attains a velocity after the collision i.e. orthogonal to the equatorial plane given as

$$v_\perp = \sqrt{(\mathcal{E}^2 - \mathcal{E}_o^2) \frac{\rho_o}{\rho_o - 1}}. \quad (38)$$

We examine the motion of the particle after collision, initially orbiting in the ISCO. The dimensionless forms of the angular momentum and magnetic field represented as ℓ and b ,

respectively are given below [4]: $\frac{dU}{d\rho} = U' = 0$ and $\frac{d^2U}{d\rho^2} = U'' = 0$ are used to find ℓ and b ,

$$U'_{\text{eff}} = \frac{1}{\rho^2(\rho-1)^2} \left[-\ell^2 \left(1 - \frac{1}{\rho}\right)^{2\nu} (2\rho - 1 - 2\nu) - 2\ell b(\rho-1) \left(1 - \frac{1}{\rho}\right)^\nu \rho\nu + \rho(\rho-1)(b^2\rho(1-3\rho+2\rho^2) + \nu(1 - \frac{1}{\rho})^\nu) \right], \quad (39)$$

$$U''_{\text{eff}} = \frac{1}{\rho^3(\rho-1)^3} \left[2\ell b(\rho-1) \left(1 - \frac{1}{\rho}\right)^\nu \rho\nu(2\rho-1-\nu) + \rho(\rho-1)(2b^2\rho^2(\rho-1)^2 + (1 - \frac{1}{\rho})^\nu \nu(1-2\rho+\nu)) + 2\ell^2 \left(1 - \frac{1}{\rho}\right)^{2\nu} (1+3\rho^2+3\nu+2\nu^2-3\rho(1+2\nu)) \right]. \quad (40)$$

Equating Eq. (39) and Eq. (40) to zero, and solving them simultaneously gives

$$\ell = \pm \sqrt{\frac{-b^2(\rho_o-1)^2\rho_o^2(1+6\rho_o^2+\nu-2\rho_o(3+\nu))}{(1-\frac{1}{\rho_o})^{2\nu}(1+2\rho_o^2+3\nu+2\nu^2-2\rho_o(1+3\nu))}}, \quad (41)$$

$$b = \sqrt{\frac{-(1-\frac{1}{\rho_o})^{\nu-1}\nu(1+2\rho_o^2+3\nu+2\nu^2-2\rho_o(1+3\nu))}{2\rho_o^2(-1+8\rho_o^3-3\nu-2\nu^2-2\rho_o^2(6+7\nu)+2\rho_o(3+7\nu+2\nu^2)\pm\nu\sqrt{\Sigma})}}, \quad (42)$$

where

$$\Sigma = -[12\rho_o^4 + (1+\nu)^2(1+2\nu) - 8\rho_o^3(3+5\nu) + 4\rho_o^2(5+15\nu+6\nu^2) - 4\rho_o(2+7\nu+6\nu^2+\nu^3)]. \quad (43)$$

For $\nu = 0.8$, when $\ell > 0$ $\rho_o \in (1, 2.44]$ and when $\ell < 0$ $\rho_o \in [1.8, 2.44]$. Also, for $\nu = 0.9$, when $\ell > 0$ $\rho_o \in (1, 2.72]$ and for $\ell < 0$ $\rho_o \in [2, 2.72]$

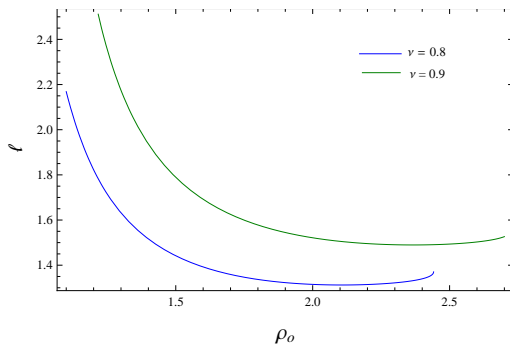


Figure 5: Angular momentum as a function of radius when $\ell > 0$.

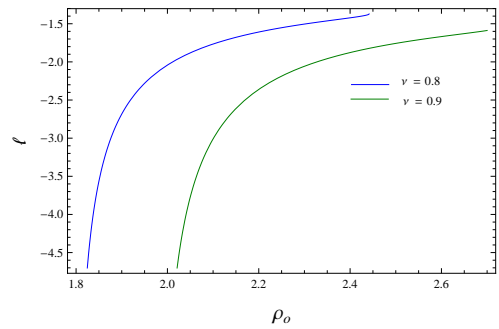


Figure 6: Angular momentum as a function of radius when $\ell < 0$.

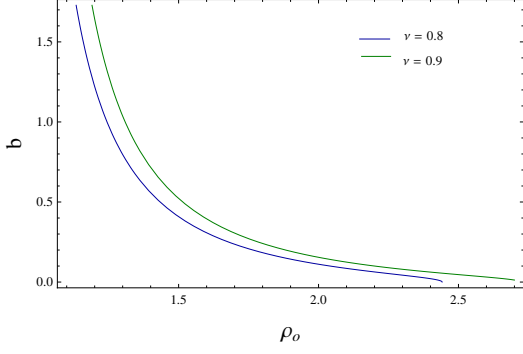


Figure 7: Magnetic field as a function of radius when $\ell > 0$.

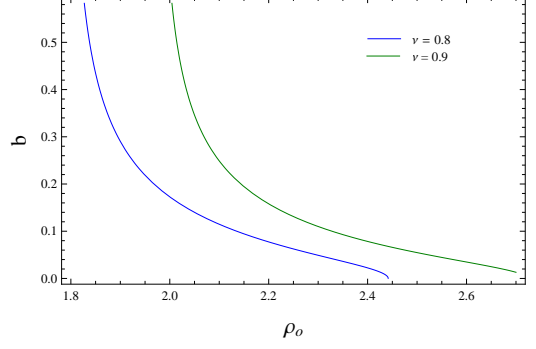


Figure 8: Magnetic field as a function of radius when $\ell < 0$.

In Fig. (5) it is shown that as the particle moves away from the naked singularity the positive angular momentum decreases. In Fig. (6) the negative angular momentum increases as a function of ρ_o . In Fig. (7) and Fig. (8) it is evident that the magnetic field strength decreases as radius of the orbit increases.

Considering the equatorial plane and utilizing the above mentioned dimensionless quantities Eqs. (29) and (30) take the form,

$$\left(\frac{d\rho_o}{d\sigma}\right)^2 = \mathcal{E}^2 - U_{\text{eff}}, \quad \frac{d\mathcal{T}}{d\sigma} = \frac{\mathcal{E}}{\left(1 - \frac{1}{\rho_o}\right)^\nu}, \quad (44)$$

$$\rho_o \frac{d\phi}{d\sigma} = \alpha, \quad \alpha = \frac{\ell}{\rho_o \left(1 - \frac{1}{\rho_o}\right)^{1-\nu}} - b\rho_o. \quad (45)$$

The effective potential given below is same as in Eq. (35) in the equatorial plane but, here we introduce α which is later used to define the Lorentz gamma factor

$$U_{\text{eff}} = \left(1 - \frac{1}{\rho_o}\right)^\nu + \left(1 - \frac{1}{\rho_o}\right) \alpha^2. \quad (46)$$

We consider a positive charged particle, so that b is positive as well. Let us suppose that the particle is moving in the circular orbit of radius r . Its momentum is given by

$$k^\mu = m\gamma(e_{(t)}^\mu + ve_{(\phi)}^\mu), \quad (47)$$

$$e_{(t)}^\mu = f^{-\nu/2} \xi_{(t)}^\mu, \quad (48)$$

$$e_{(\phi)}^\mu = r^{-1} f^{-(1-\nu)/2} \xi_{(\phi)}^\mu. \quad (49)$$

The velocity of the particle with respect to a rest frame is represented by v . Here, γ is the Lorentz gamma factor. Using the normalization condition $k^2 = -m^2$ we obtain $\gamma = (1 - v^2)^{-1/2}$. In Eqs. (48,49) $\xi_{(t)}^\mu = (1, 0, 0, 0)$ and $\xi_{(\phi)}^\mu = (0, 0, 0, 1)$ are the Killing vectors whereas $e_{(t)}^\mu$ and $e_{(\phi)}^\mu$ refers to the tetrad basis. For a positively charged particle

and $v > 0$, the Lorentz force is *repulsive* (i.e. directed outwards the naked singularity), while for $v < 0$, it is *attractive*.

Using relation $d\phi/d\tau = v\gamma/r$ one gets

$$v\gamma = \alpha. \quad (50)$$

This relation allows one to write

$$\gamma^2 = 1 + \alpha^2, \quad v = \frac{\alpha}{\sqrt{1 + \alpha^2}}. \quad (51)$$

Now we discuss the behavior of v , effective potential and the Lorentz gamma factor for $\nu = 0.8$ and $\nu = 0.9$.

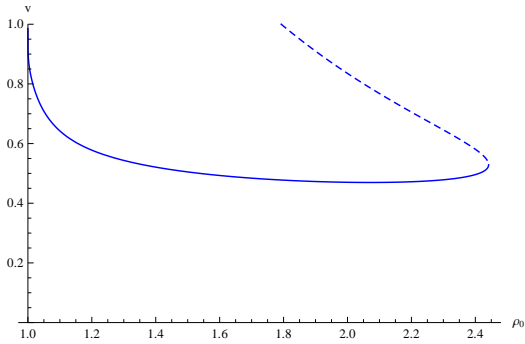


Figure 9: Velocity with respect to a rest frame for $\nu = 0.8$. Dotted curve is for $\ell < 0$ and solid curve for $\ell > 0$.

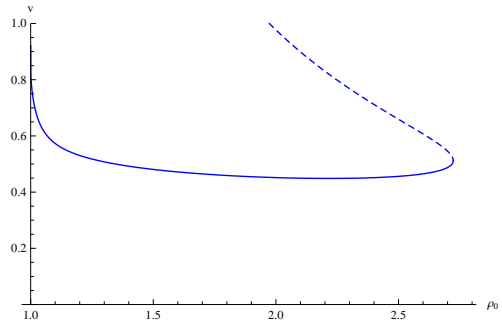


Figure 10: Velocity with respect to a rest frame for $\nu = 0.9$. Dotted curve is for $\ell < 0$ and solid curve for $\ell > 0$.

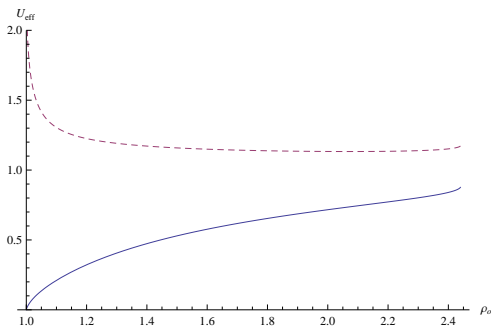


Figure 11: For $\ell > 0$ and $\nu = 0.8$, the Lorentz gamma factor (dotted graph) and U_{eff} are plotted as a function of ρ_o .

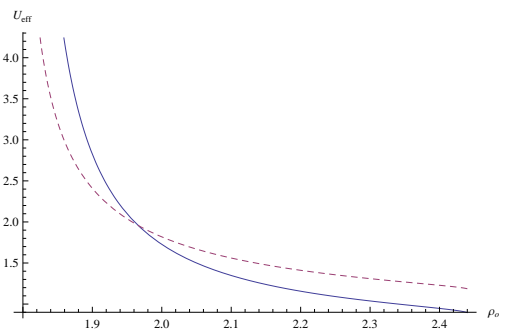


Figure 12: For $\ell < 0$ and $\nu = 0.8$, the Lorentz gamma factor (dotted graph) and U_{eff} are plotted as a function of ρ_o .

The velocity of the particle with respect to a rest frame as a function of ρ_o is shown in Figs. (9) and (10), $\nu = 0.8$ and 0.9 . It is evident that v decreases as the particle moves away from the naked singularity, both for $\ell > 0$ and $\ell < 0$. In Fig. (11) when $\ell > 0$ and

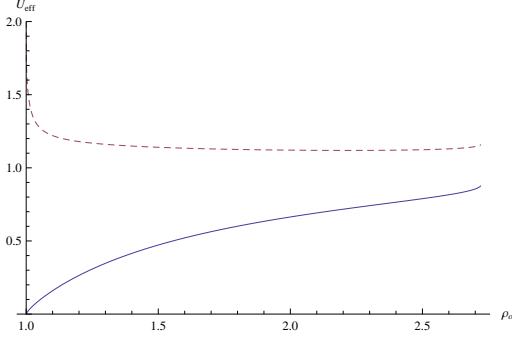


Figure 13: For $\ell > 0$ and $\nu = 0.9$, the Lorentz gamma factor (dotted graph) and U_{eff} as a function of ρ_o .

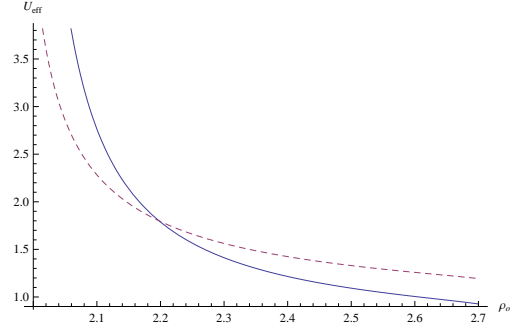


Figure 14: For $\ell < 0$ and $\nu = 0.9$, the Lorentz gamma factor (dotted graph) and U_{eff} as a function of ρ_o .

$\nu = 0.8$, U_{eff} monotonically decreases from its value 0.88 at $\rho_o = 2.44$ till it reaches $\rho_o = 1$. The Lorentz gamma factor γ at $\rho_o = 2.44$ is 1.2. In Fig. (12) for $\ell < 0$ and $\nu = 0.8$ both the functions rise to infinity at $\rho_o = 1.8$. In Fig. (13) considering $\ell > 0$ and $\nu = 0.9$, U_{eff} and γ exhibit the same behavior as described above for $\nu = 0.8$, but for different values of ρ_o . Both the functions infinitely grow at $\rho_o = 2$ when $\ell < 0$ as shown in Fig. (14).

4.2.1 Energy of the particle at ISCOs

The energy of the particle present in the ISCO for different values of ν is demonstrated in Figs. (15,16). If the Lorentz force acting on the particle is repulsive i.e., $\ell > 0$, then the energy possessed by the particle is minimum as compared to the particle experiencing an attractive Lorentz force i.e., $\ell < 0$. It is also observed that with the increasing value of ν , the energy of the particle decreases when $\ell > 0$ and increases when $\ell < 0$.

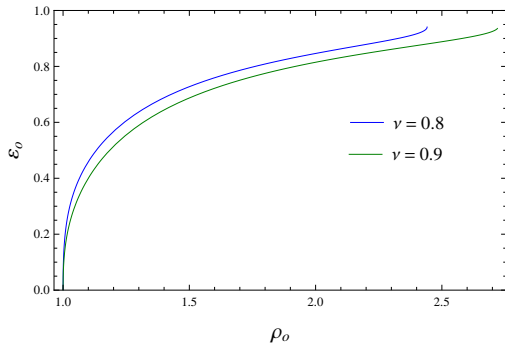


Figure 15: Energy of the particle for $\ell > 0$.

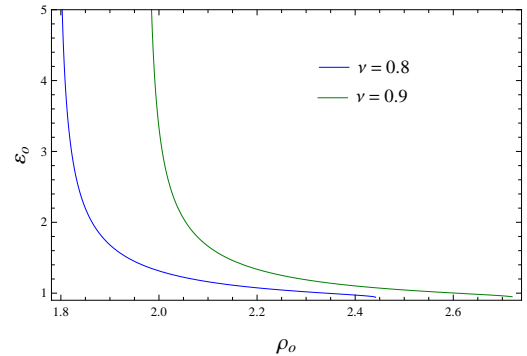


Figure 16: Energy of the particle for $\ell < 0$.

4.2.2 Escape trajectories and escape velocity

In order to visualize the escape trajectories of the ejected particle initially present in the ISCO, Eqs. (32,33) are numerically solved in Mathematica using NDSolve command by keeping the radial velocity zero after collision. Figs. (18,20) display the path followed by the particle after being kicked from the ISCO, that ultimately escapes to infinity. Figs. (17,19) show capture by the naked singularity after the collision. Utilizing the Eqs. (34-38) the escape velocity is estimated from the numerical results, obtained from the numerical integration of the dynamical equations [6]. The escape velocity for different values of ν is illustrated in Figs. (21,22). With the increasing value of ν the escape velocity of the particle increases.

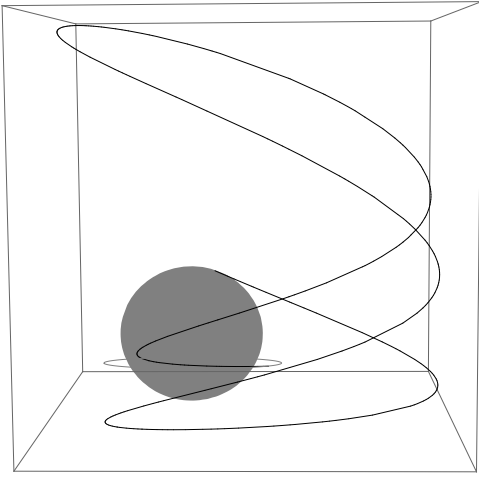


Figure 17: Escape trajectory for $\nu = 0.9$, $\ell = 1.49355$, $b = 0.0464893$, $\rho_o = 2.5$ and $\mathcal{E} = 1.16884$.

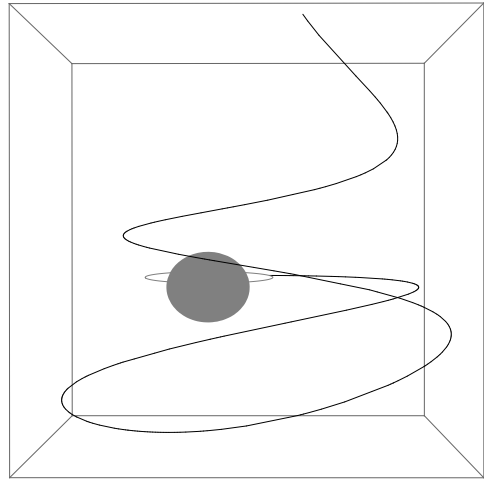


Figure 18: Escape trajectory for $\nu = 0.9$, $\ell = 1.50555$, $b = 0.124502$, $\rho_o = 2.1$ and $\mathcal{E} = 1.16971$.

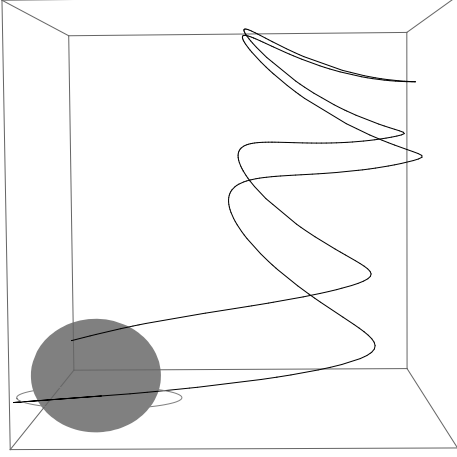


Figure 19: Escape trajectory for $\nu = 0.9$, $\ell = -1.75741$, $b = 0.0547023$, $\rho_o = 2.5$ and $\mathcal{E} = 1.082$.

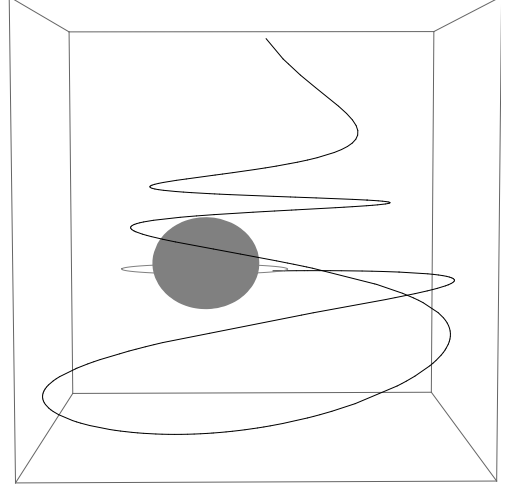


Figure 20: Escape trajectory for $\nu = 0.9$, $\ell = -2.05737$, $b = 0.109975$, $\rho_o = 2.3$ and $\mathcal{E} = 1.19955$.

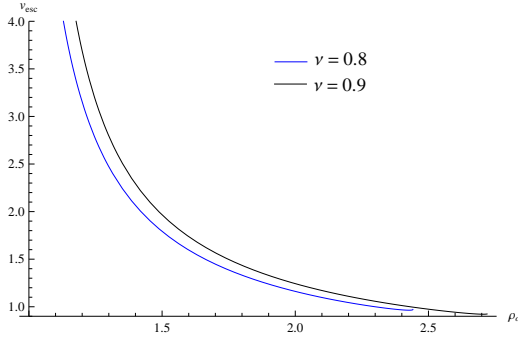


Figure 21: Escape velocity for $\ell > 0$.

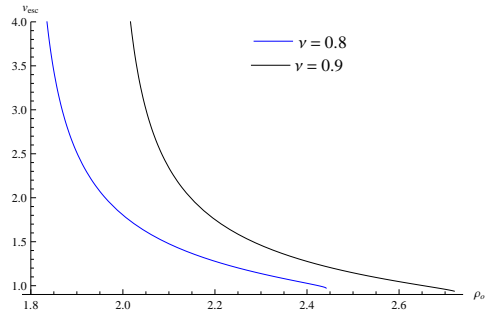


Figure 22: Escape velocity for $\ell < 0$.

5 Particle collision at ISCO

Let us consider a collision between two particles with the same mass m and opposite charges, moving along the same circular orbit in the opposite directions. The four-momentum of the particles is given as under,

$$k_1^\mu = m\gamma(e_{(t)}^\mu + ve_{(\phi)}^\mu), \quad k_2^\mu = m\gamma(e_{(t)}^\mu - ve_{(\phi)}^\mu), \quad (52)$$

$$K^\mu = k_1^\mu + k_2^\mu = 2m\gamma e_{(t)}^\mu. \quad (53)$$

K^μ is the four-momentum of the system after the collision. Let us denote the center-of-mass energy after the collision by \mathcal{M} ,

$$\mathcal{M}^2 = -K^\mu K_\mu = -g_{\mu\delta} K^\mu K^\delta = (2m\gamma)^2, \quad \mathcal{M} = 2m\gamma. \quad (54)$$

It is obvious that the center-of-mass energy \mathcal{M} depends on the Lorentz gamma factor, as the value of γ increases the energy generated as a result of the collision is maximum. In Fig. (11) when $\ell > 0$ and $\nu = 0.8$, γ remains close to 1. In this case, the energy produced is not significantly large. In Fig. (12) when $\ell < 0$, γ rises to infinity at $\rho_o=1.8$. Hence, a large amount of energy can be obtained in the presence of a weak magnetic field if the particle experiences an attractive Lorentz force. We can also examine the energy generated for $\nu = 0.9$. It exhibits the same behavior as for $\nu = 0.8$, but for different values of ρ_o .

6 Conclusion

In this paper, we established an analysis to investigate the escape velocity of the particle initially orbiting in the ISCO of a magnetized JNW naked singularity. The escape trajectories followed by the particle after the collision are analyzed utilizing the dynamical equations. The particle may either escape to infinity, captured by the naked singularity or will continue a bounded motion after the collision. Also, the center of mass energy is obtained as a result of the collision between two particles having the same mass and opposite charges, moving along the same circular orbit in the opposite directions. It is observed that the maximum amount of energy can be achieved depending upon the Lorentz gamma factor.

References

- [1] J. C. McKinney and R. Narayan, “*Disk-Jet Coupling in Black Hole Accretion Systems II: Force-Free Electrodynamical Models*”, Mon. Not. Roy. Astron. Soc. **375** (2007) 531, [[astro-ph/0607576](#)].
- [2] R. Narayan, J. E. McClintock, and A. Tchekhovskoy, “*Energy Extraction from Spinning Black Holes via Relativistic Jets*”, [arXiv:1303.3004](#).
- [3] I. A. U. Symposium, K. Strassmeier, A. Kosovichev, J. Beckman, and I. A. Union, *Cosmic Magnetic Fields (IAU S259): From Planets to Stars and Galaxies*. IAU symposium and colloquium proceedings series. Cambridge University Press, 2009.
- [4] V. P. Frolov and A. A. Shoom, “*Motion of charged particles near weakly magnetized Schwarzschild black hole*”, Phys. Rev. D **82** (2010) 084034, [[arXiv:1008.2985](#)].
- [5] V. P. Frolov, “*Weakly magnetized black holes as particle accelerators*”, Phys. Rev. D **85** (2012) 024020, [[arXiv:1110.6274](#)].

- [6] A. A. Zahrani, V. P. Frolov, and A. A. Shoom, “*Critical escape velocity for a charged particle moving around a weakly magnetized Schwarzschild black hole*”, Phys. Rev.D **87** (2013) 084043, [[arXiv:1301.4633](#)].
- [7] Y. Nakamura and T. Ishizuka, “*Motion of a charged particle around a black hole permeated by magnetic field and its chaotic characters*”, Astrophys. Space Sci. **210** (1993) 105.
- [8] M. Takahashi and H. Koyama, “*Chaotic motion of Charged Particles in an Electromagnetic Field Surrounding a Rotating Black Hole*”, Astrophys. J. **693** (2009) 472, [[arXiv:0807.0277](#)].
- [9] O. Kopacek, V. Karas, J. Kovar, and Z. Stuchlik, “*Transition from Regular to Chaotic Circulation in Magnetized Coronae near Compact Objects*”, Astrophys. J. **722** (2010) 1240, [[arXiv:1008.4650](#)].
- [10] O. Kopacek, J. Kovar, V. Karas, and Z. Stuchlik, “*Recurrence plots and chaotic motion around Kerr black hole*”, AIP Conf. Proc. **1283** (2010) 278, [[arXiv:1011.2707](#)].
- [11] G. Preti, “*Nonequatorial charged particle confinement around Kerr black holes*”, Phys. Rev. D **81** (2010) 024008.
- [12] V. P. Frolov and P. Krtous, “*Charged particle in higher dimensional weakly charged rotating black hole spacetime*”, Phys. Rev. D **83** (2011) 024016, [[arXiv:1010.2266](#)].
- [13] T. Igata, T. Koike, and H. Ishihara, “*Constants of Motion for Constrained Hamiltonian Systems: A Particle around a Charged Rotating Black Hole*”, Phys. Rev. D **83** (2011) 065027, [[arXiv:1005.1815](#)].
- [14] D. Pugliese, H. Quevedo, and R. Ruffini, “*Motion of charged test particles in Reissner-Nordstrom spacetime*”, Phys. Rev. D **83** (2011) 104052, [[arXiv:1103.1807](#)].
- [15] U. Yurtsever, “*Geometry of chaos in the two center problem in general relativity*”, Phys. Rev. D **52** (1995) 3176, [[gr-qc/9412031](#)].
- [16] C. Dettmann, N. Frankel, and N. Cornish, “*Fractal basins and chaotic trajectories in multi - black hole space-times*”, Phys. Rev. D **50** (1994) 618–621, [[gr-qc/9402027](#)].
- [17] M. Jamil, S. Hussain, and B. Majeed, “*Dynamics of Particles Around a Schwarzschild-like Black Hole in the Presence of Quintessence and Magnetic Field*”, Eur. Phys. J. C **75** (2015) 24, [[arXiv:1404.7123](#)].

- [18] S. Hussain, I. Hussain, and M. Jamil, “*Dynamics of a Charged Particle Around a Slowly Rotating Kerr Black Hole Immersed in Magnetic Field*”, *Eur. Phys. J. D* **74** (2014) 3210, [[arXiv:1402.2731](#)].
- [19] K. Virbhadra, D. Narasimha, and S. Chitre, “*Role of the scalar field in gravitational lensing*”, *Astron. Astrophys.* **337** (1998) 1, [[astro-ph/9801174](#)].
- [20] K. S. Virbhadra and G. F. R. Ellis, “*Gravitational lensing by naked singularities*”, *Phys. Rev.D* **65** (2002) 103004.
- [21] K. Virbhadra and C. Keeton, “*Time delay and magnification centroid due to gravitational lensing by black holes and naked singularities*”, *Phys. Rev.* **77** (2008) 124014, [[arXiv:0710.2333](#)].
- [22] I. Fisher, “*Scalar mesostatic field with regard for gravitational effects*”, *Zh. Eksp. Teor. Fiz.* **18** (1948) 636, [[gr-qc/9911008](#)].
- [23] A. I. Janis, E. T. Newman, and J. Winicour, “*Reality of the Schwarzschild Singularity*”, *Phys. Rev. Lett.* **20** (1968) 878.
- [24] M. Wyman, “*Static Spherically Symmetric Scalar Fields in General Relativity*”, *Phys. Rev. D* **24** (1981) 839.
- [25] A. Agnese and M. La Camera, “*Gravitation without black holes*”, *Phys. Rev. D* **31** (1985) 1280.
- [26] M. D. Roberts, *Scalar Field Counterexamples to the Cosmic Censorship Hypothesis*, *Gen. Rel. Grav.* **21** (1989) 907.
- [27] K. S. Virbhadra, “*Janis-Newman-Winicour and Wyman solutions are the same*”, *Int. J. Mod. Phys. A* **12** (1997) 4831, [[gr-qc/9701021](#)].
- [28] A. Janis, D. Robinson, and J. Winicour, “*Comments on einstein scalar solutions*”, *Phys. Rev.* **186** (1969) 1729.
- [29] B. C. Xanthopoulos and T. Zannias, “*Einstein Gravity Coupled to a Massless Scalar Field in Arbitrary Space-time Dimensions*”, *Phys. Rev. D* **40** (1989) 2564.
- [30] S. Abdolrahimi and A. A. Shoom, “*Analysis of the Fisher solution*”, *Phys. Rev. D* **81** (2010) 024035, [[arXiv:0911.5380](#)].
- [31] S. S. Yazadjiev, “*Uniqueness of the static spacetimes with a photon sphere in Einstein-scalar field theory*”, *Phys. Rev. D* **91** (2015) 123013, [[arXiv:1501.06837](#)].

- [32] A. N. Chowdhury, M. Patil, D. Malafarina, and P. S. Joshi, “*Circular geodesics and accretion disks in Janis-Newman-Winicour and Gamma metric*”, Phys. Rev. D **85** (2012) 104031, [[arXiv:1112.2522](#)].
- [33] M. Patil and P. S. Joshi, “*Acceleration of particles in Janis-Newman-Winicour singularities*”, Phys. Rev. D **85** (2012) 104014, [[arXiv:1112.2525](#)].
- [34] R. Penney, “*Axially symmetric zero-mass meson solutions of Einstein equations*”, Phys. Rev. **174** (1968) 1578.
- [35] M. Astorino, “*Embedding hairy black holes in a magnetic universe*”, Phys. Rev. D **87** (2013) 084029, [[arXiv:1301.6794](#)].
- [36] M. Astorino, “*C-metric with a conformally coupled scalar field in a magnetic universe*”, Phys. Rev. D **88** (2013) 104027, [[arXiv:1307.4021](#)].
- [37] R. Shiose, M. Kimura, and T. Chiba, “*Motion of Charged Particles around a Weakly Magnetized Rotating Black Hole*”, Phys. Rev. D **90** (2014) 124016, [[arXiv:1409.3310](#)].
- [38] Q.-H. Huang, J.-H. Chen, and Y.-J. Wang, “*Chaotic Motion of a Charged Particle around a Weakly Magnetized Schwarzschild Black Hole Containing Cosmic String*”, Chin. Phys. Lett. **31** (2014) 060402.
- [39] Y.-K. Lim, “*Motion of charged particles around a magnetized/electrified black hole*”, Phys. Rev. D **91** (2015) 024048, [[arXiv:1502.00722](#)].
- [40] B. K. Harrison, “*New Solutions of the Einstein-Maxwell Equations from Old*”, J. Math. Phys. **9** (1968).
- [41] F. Dowker, J. P. Gauntlett, D. A. Kastor, and J. H. Traschen, “*Pair creation of dilaton black holes*”, Phys. Rev. D **49** (1994) 2909, [[hep-th/9309075](#)].
- [42] M. Ortaggio, “*Higher dimensional black holes in external magnetic fields*”, JHEP **0505** (2005) 048, [[gr-qc/0410048](#)].
- [43] N. Dadhich, C. Hoenselaers, and C. V. Vishveshwara, “*Trajectories of charged particles in the static Ernst space-time*”, J. Phys. A **12** (1979) 215.
- [44] E. Esteban, “*Geodesics in the Ernst metric*”, Nuovo Cimento B **79** (1984) 76.
- [45] V. Karas and D. Vokrouhlicky, “*Test particle motion around a magnetised Schwarzschild black hole*”, Class. Quant. Grav. **7** (1990) 391.